Polymer Testing 104 (2021) 107378

Contents lists available at ScienceDirect

Polymer Testing

journal homepage: www.elsevier.com/locate/polytest

Characterising the friction coefficient between rubber O-rings and a rigid surface under extreme pressures

Eduardo Yanes [a,*], Nicola M. Pugno [b,a], Julien Ramier [c], Benjamin Berryhill [d], James JC. Busfield [a]

[a] Soft Matter Group, School of Engineering & Materials Science, Queen Mary University of London, Mile End Road, London, E1 4NS, United Kingdom
[b] Laboratory of Bio-Inspired, Bionic, Nano, Meta Materials & Mechanics, Department of Civil, Environmental, and Mechanical Engineering, University of Trento, Via Mesiano 77, 38123, Trento, Italy
[c] Schlumberger Cambridge Research Ltd, UK
[d] Materials, Modeling, & Mechanical Technologies, Schlumberger, 200 Gillingham Lane, Sugar Land, TX, 77478, United States

ARTICLE INFO

Keywords:
Rubber
Friction
High pressure
Fluoroelastomer
Experiment

ABSTRACT

Previous research into the friction behaviour of elastomers has typically focused on the effects of velocity, contact pressure, counter surface and lubrication on the coefficient of friction. O-ring type elastomer seals are common in many different industries. Friction plays a critical role during the setting and in service of these components. An experimental O-ring friction testing rig has been developed that can measure the effects of sliding speed and hydrostatic pressure on elastomer friction. Finite element analysis (FEA) packages can adopt fixed friction coefficients or ones that are pressure dependent. For the latter case, the dependence of the frictional behaviour is typically obtained from the instantaneous stress response at any given pressure and then related to the normal force response. The friction rig described in this paper uses industry standard dimensions for the O-ring gland, the pre-compression levels, extrusion gap size and pressure rating. The coefficient of friction is derived by dividing the measured friction force by the normal force, which was determined using an FEA modelling approach, as it could not be measured directly. Finally, a relationship between the frictional velocity and surface roughness is obtained in order to provide a frequency dependent Coefficient of Friction (CoF) that is easily translatable between surfaces.

1. Introduction

The mechanical properties of elastomers and how they change under a hydrostatic pressure has been studied previously [1]. It is understood that high pressure reduces the polymer chain mobility which increases the effective elastic modulus of the material. This modulus increase can significantly change the sealing effectiveness. But the change in stiffness is not only pertinent to the quasi-static behaviour, it also plays a large role on the dynamic properties and, as a consequence, on the resulting frictional properties [7,8,14,23]. Because elastomer friction is heavily dependent on the viscoelastic behaviour of the material, this behaviour becomes particularly important in dynamic seals, which are subjected to continuous frictional sliding in service.

Pressure increase for frictional studies has always taken place with a direct load on the elastomer; this works well when the pressure range does not cause changes in the glass transition temperature (T_g) or the elastic modulus of the material. However, oilfield conditions require seals to have service pressure ratings upwards of 70 MPa [15]. Use of regular indenters or normal forces at these pressures will cause severe problems such as the puncturing or fracture of the sample resulting from very large local deformations. If extreme pressures are to be applied to the elastomer, they must be applied in heavily constrained conditions. In practice O-ring seals are used in these high fluid pressure conditions, which also makes them ideal for this investigation.

There are many experimental methods that can be used to obtain a coefficient of friction (CoF) for an elastomer sliding against a contact surface, yet high pressure conditions are not typically employed. When it comes to large elastomeric seals, such as the ones used in the oilfield, prototype build-and-then-test design validation methods are expensive and slow, which means FEA techniques have become widely adopted. In order to validate models of elastomer sliding friction under the conditions of a large hydrostatic pressure, a new experimental methodology

* Corresponding author.
E-mail address: efyn66@gmail.com (E. Yanes).

https://doi.org/10.1016/j.polymertesting.2021.107378
Received 17 February 2021; Received in revised form 10 September 2021; Accepted 11 October 2021
Available online 12 October 2021

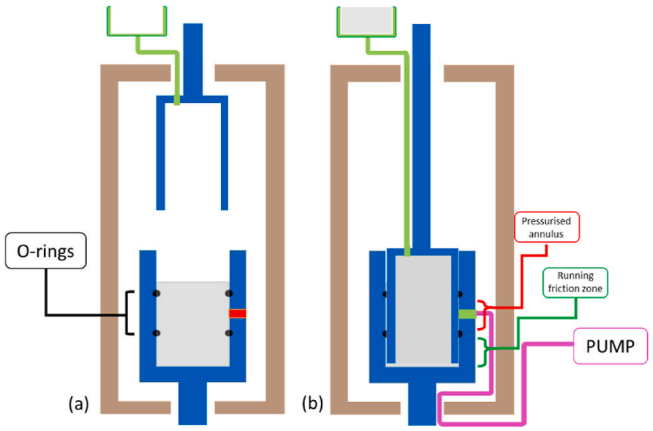

Fig. 1. Experimental apparatus for rubber O-ring friction under extreme pressure. (a) Cut away cross-section of the novel friction rig 3D model prior to engaging the seals. (b) After the seal has been engaged. The diagram highlights that the full working friction rig is located inside an environmental chamber to allow the operating temperature to be controlled.

has been developed and is reported here.

Research into the frictional behaviour of O-ring seals, whether by industry [2] or academic research [3] does analyse the behaviour of O-ring friction under pressure and different speeds. Typically, this velocity change is not related to the surface roughness (frequency dependency). Even with these changes in speed and pressure, frictional behaviour tends to be described simply as different constant values that change with different velocities. The intent of this paper is to check the validity of a testing method that can describe the change in O-ring friction with relation to surface roughness related to speed at different pressure levels and temperatures. The method needs a liquid environment for pressurisation.

2. Materials

All O-rings used for the experiments were made using a commercial highly filled fluoroelastomer rubber supplied by Parker (FKM 90 ShA). The pressurised fluid was a Silicone Oil supplied by Sigma Aldrich, which acted not only as a hydraulic pressurisation medium but also as a lubricant. The characterisation of the mechanical properties of the elastomer was performed using an Instron 5900R84 fitted with a 500 N load cell. Quasi-static tension and compression tests were made using dumbbell shaped samples and cylindrical buttons, respectively. Tensile testing strain data was obtained with a video-extensometer to ensure grip slippage does not influence the data acquisition. Results of stress-strain experiments were fitted using the SEF curve fitting algorithm within Abaqus to obtain the coefficients for the Yeoh model.

3. Experimental method

For the current work, a sleeve-piston type of rig was built that could withstand an internal pressurisation of up to 35 MPa whilst running friction tests as shown in Fig. 1. At these high pressures, during the experiment, neither the normal pressures nor the contact area were easy to measure directly, so both had to be calculated using a finite element analysis (FEA) model.

The rig is based on a simple piston design (Fig. 1), in which the sleeve will hold O-rings that can vary in cross-sectional diameter and compression levels, with a rod (hollowed for ease of handling) that varies in surface roughness characteristics. The surface profile effects on rubber friction are well known [4–6,16] so the piston is characterised with profilometry and analysed with a height difference correlation function (HDC). Profilometry of the surface characteristics of the piston was done using a Mitutoyo SJ-400 profilometer.

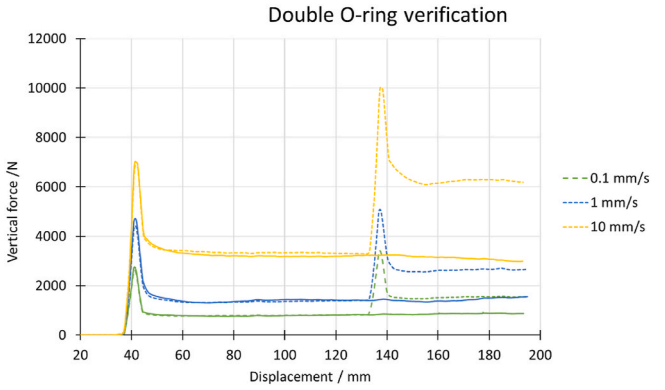

Fig. 2. Piston setting tests, continuous lines represent the measured insertion force when a single O-ring is fitted into the rig. Dashed lines shows the measured force when both O-rings are in position. The force contribution from the second O-ring is simply double the magnitude when a single O-ring is used.

The upper section (piston) is mobile and engages with the fixed section (sleeve); both sections are designed to connect to Instron ½ inch female connection type. The mobile section connects to the crosshead of the 5900R84 tension machine; this provides control of the speed for testing (user defined in the range of 0.1–10 mm/s) and a load cell that can read the vertical forces generated by the friction once it engages an O-ring. The fixed section has O-ring glands that can fit two different sized O-rings with two different compression levels (13% and 24% nominal compression). The defined dimensions allow a compromise to be made between ease of handling without the requirement to use any particular lifting tools to assemble the rig, whilst ensuring that the piston is able to safely withstand the large stresses encountered during testing. The glands are repeated to create a sealed volume between two O-rings. Between the two rings is located a pressure injection point which allows the pressure between the two seals to be increased to a known level.

There is the assumption of equal contribution to the frictional forces by both O-rings. Even with precautions, there is the risk of decentralisation of the piston, which can cause damage or uneven force responses. In order to test the validity of this assumption, tests were run at different speeds where only one O-ring was in position and another set of tests were done with both O-rings in place. Tests were carried out without any form of lubricant and thus, no pressure application. Fig. 2 shows that the assumption of basically equal contribution to friction by both O-rings is valid; thus the final frictional value of two O-rings is equal to double the single O-ring value. The initial setting response is slightly lower for the second O-ring; this could be attributed to centralisation effects, with the first O-ring correcting for the majority of any eccentricity issues that stem from the initial misalignment of the testing equipment.

After both O-rings are fully engaged, pressurisation causes the upper O-ring to be pushed upwards and the lower one to be pushed downwards. As a result of this symmetry, any direction of motion can be used to study the frictional response since effects like extrusion or shear forces on the O-rings will cancel each other out. For example, the lower O-ring is sheared downwards by the pressurised fluid, which might result in a negative contribution to the piston's upwards movement; this is countered by the upper O-ring creating an identical but opposite shear. The gland design and interference fit were designed to ensure that specified compression levels could be obtained for each O-ring. When no pressurisation fluid was used in the test, the difference in compression levels was large enough that two distinctly different contact pressures could be studied. The Parker Handbook for O-rings [15] was used to specify the detailed dimensions for the O-Ring glands and their machined surface characteristics, such as surface roughness and tapering dimensions.

In order to avoid any form of trapped gas between the sealing components, the sleeve was first filled with the testing fluid up to the position of the top seal and the elastomer O-rings were placed in their

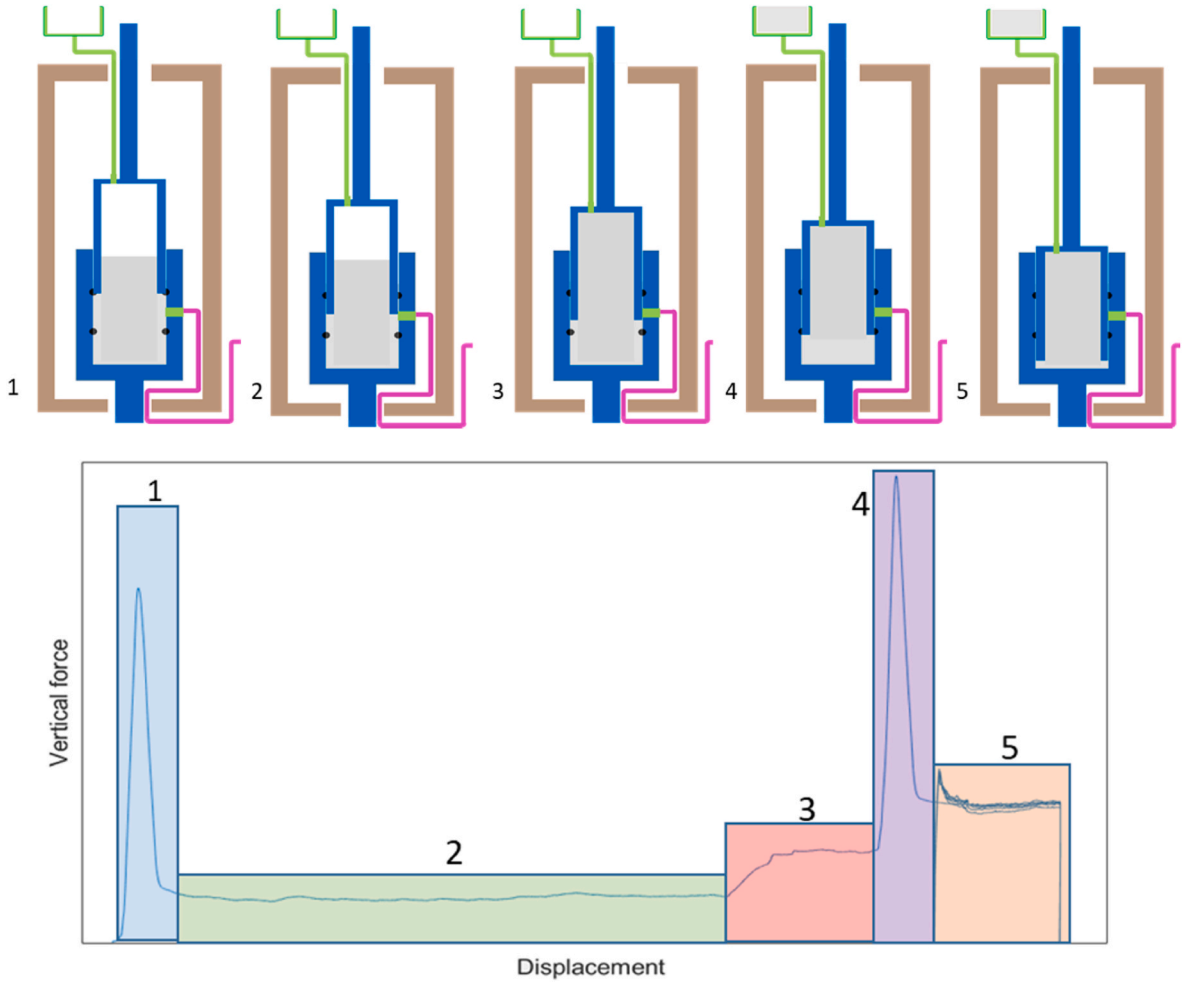

Fig. 3. The typical force output from the friction rig can be represented in 5 distinct sections. 1: piston engagement of the first O-ring. 2: running friction forces whilst the piston travels down the sleeve. 3: Upward forces generated by the fluid entering the pipes that lead to the overhead tank (silicone oil for this case). 4: piston engagement with the second O-ring, the annular seal is created. 5: running friction tests that can be pressurised (this is the standard data collection region).

desired positions. When the piston was lowered, the air and excess fluid escaped through two 8 mm holes drilled on the top part of the piston, which then flowed into an overhead tank at atmospheric pressure. The tank holds the fluid while the piston is engaged and then returns it back into the system when the piston ascends. The holes were as large as possible to maintain the strength of the piston and also to minimise the pressure drop when using high viscosity fluids. The additional forces that would be generated as a consequence of any upwards fluid flow could be accounted for using the Hagen-Poiseuille equation:

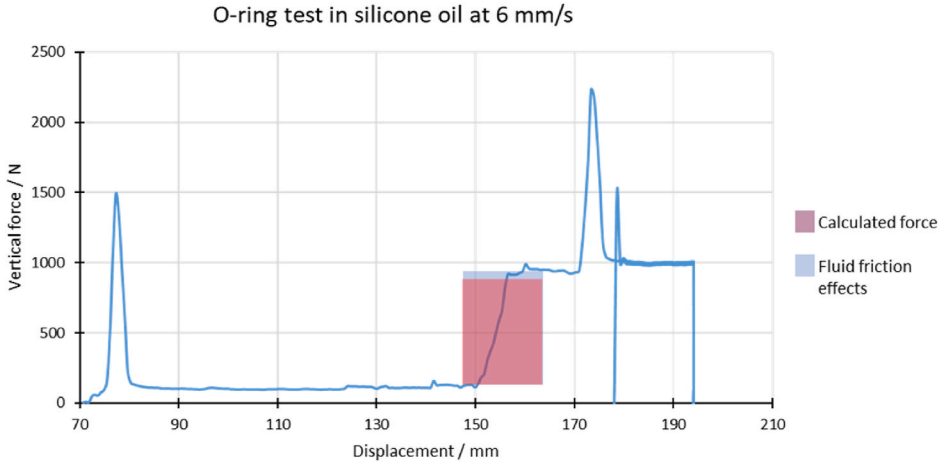

Fig. 4. Fluid resistance effects on the vertical forces that occur during the experiments. The observed force is subtracted from the total value of running friction in order to read the elastomer friction contribution.

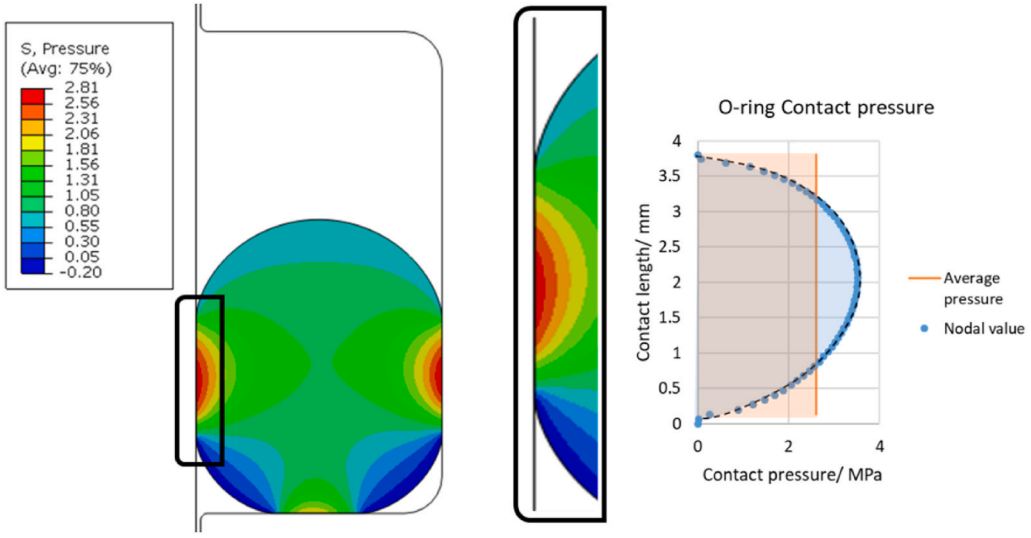

Fig. 5. An O-ring compressed axisymmetric model used to calculate the normal forces and contact pressures encountered during installation. The right hand graph presents the difference between the local pressure (where each point represents the force imposed on a node) and the equivalent average pressure level between the linear elements. The areas under the blue curve and the orange curve are equal. All stress values are given in MPa. (For interpretation of the references to colour in this figure legend, the reader is referred to the Web version of this article.)

$$\Delta P = \frac{Q8L\eta}{\pi R^4} \tag{1}$$

where ΔP is the pressure differential, Q is the flowrate in the pipe, L is the length of the pipe, η is fluid viscosity, and R is the pipe radius. Clearly, increasing the radius produced the most significant way to decrease the pressure drop (e.g. a doubling of the radius reduces the pressure build-up by a factor of 16). The piston was fitted with two pipes of 1.8 mm inner radius connecting to an overhead tank in order to contain the fluid. For silicone oil testing at 20 °C, 6 mm/s vertical velocity, with a length of pipes roughly 1 m long, the force increase is calculated as 751 N. Fig. 4 shows an increase in force that is approximately 800 N, which is reasonable given the potential of additional frictional effects inside the pipes. Silicone oil can be considered a Newtonian fluid at this shear rate with a constant viscosity [9]. Although equation (1) can provide a reasonable calculation for its contribution to the vertical force, it is not used here. The raw values of fluid upwards force are directly observed during the experiment and the additional contribution is easily subtracted from the total vertical force observed. Equation (1) was used specifically during the design of the rig to avoid excessive forces from the pressurised fluid.

Fig. 3 shows a how the force varies with displacement in a typical experiment as the cylinder is assembled. The graph is divided into distinct 5 regions, as in Fig. 3. As the piston goes down into the sleeve, it initially has no resistance. Once the piston reaches the O-ring, it compresses it to fill the gland and a large spike in the force is observed (Region 1). After setting, the vertical force arises only from the sliding friction of the O-Ring sliding against the rod (Region 2). Region 3 is where fluid flowing to the overhead tank generates an additional upward force that must be accounted for when analysing the running friction forces. Region 4 is the engagement of the second O-ring, at this point the annular seal is created. Region 5 results are the ones taken for the running friction forces as the piston is cycled up and down.

Despite a large volume of fluid being required to fill the chamber, the amount of pressurised fluid in the gap between the O-ring seal and the piston is slightly less than 90 ml, thus, a high capacity pump is not required. A 35 MPa rated pump is connected to the midpoint of the sleeve; once the seal is complete, pressurisation takes place and the pump is set to maintain a constant pressure. Leaks can be detected by monitoring flow, at no point were leaks observed in the pressurisation part of the system. Motion of the piston begins once the pump flowrate is reduced to less than 0.05 ml/min. At no point during testing was there any indication of a leak, either by a change in flowrate or by fluid leaking from the top or the bottom of the seal. Because oilfield pressure ratings are typically specified in imperial units, the pressurisation occurs with reference to values that are in hundreds of pounds per square inch (psi). Pressure levels are as follows: atmospheric, 100 psi, 200 psi, up to 500 psi (which is in increment of 0.69 MPa), 1000 psi, 1500 psi … 5000 psi (which is an increment of 3.45 MPa up to 35 MPa). The results are plotted consistently throughout using SI units.

Surface roughness coefficients such as the Hurst exponent H, horizontal ($\xi_{\parallel}$) and vertical ($\xi_{\perp}$) cut-off lengths were obtained using the Height Difference Correlation function (HDC). This method is commonly used for random surface characterisation such as roads [16,26,29] or chemically abraded surfaces [10,11]. HDC function equation (equation (2)) is presented as:

$$C(\lambda) = < (z(x+\lambda) - z(x))^2 >_x \tag{2}$$

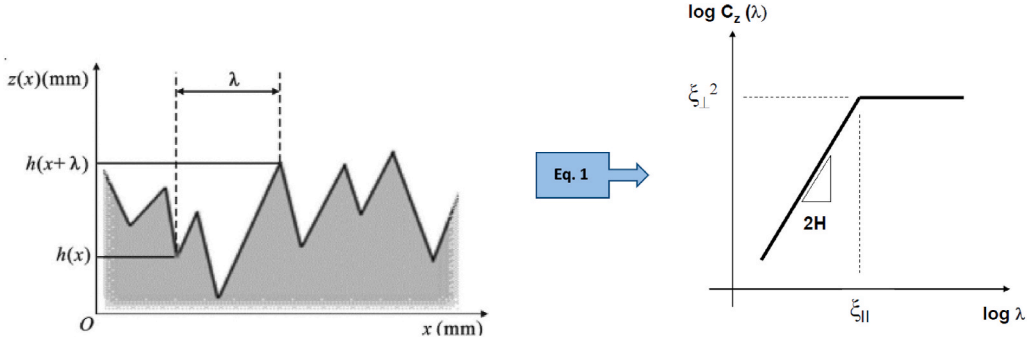

Fig. 6. Height Difference Correlation (HDC) function explained in order to determine surface parameters.

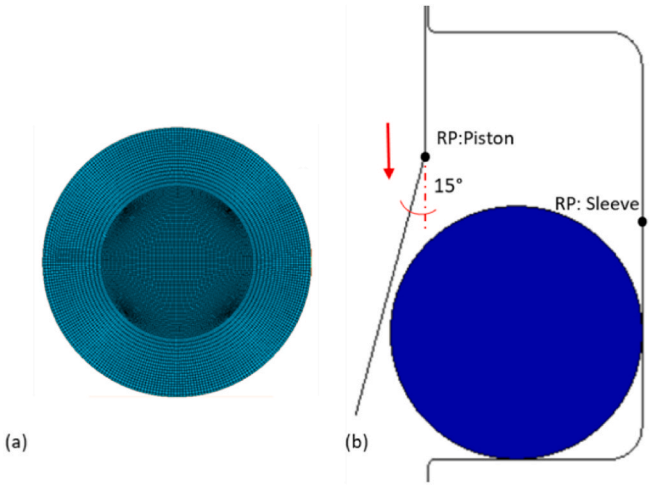

Fig. 7. (a) mesh for the O-ring axisymmetric model. (b) setting step of the simulation. The sleeve reference point is fixed in all directions and rotations. The piston reference point is fixed in the X and Z direction, it moves downwards until the seal is made.

where z is the height of the surface profile along a horizontal position x and λ are the horizontal distance between the points observed. The results are averaged and λ is further increased. When the $C(\lambda)$ versus λ is plotted on a log-log graph, the slope of the curve before the plateau is related to the Hurst parameter H by a factor of 2 (as is shown in Fig. 6). Results from HDC function characterisation are presented in the experimental results section.

4. Finite element modelling & validation

All of the FEA data presented were calculated using Abaqus v6.14. The normal pressure response was calculated using an FEA axisymmetric model (Fig. 5) that adopted a simple stored energy function (SEF) approach where the rubber, a fluoroelastomer (FKM), was characterised in both tension and compression. The Yeoh [18] model fit of the stress strain behaviour in both tension and compression is presented in Fig. 8. Both the sleeve and the piston were steel made and modelled as analytical rigid surfaces because of their large difference in elastic moduli when compared to that of the elastomer; this simplified the model and saved computational effort. The elastomer component used hybrid elements and enhanced hourglass control. Quad shaped elements with structured technique are used (seen in Fig. 7) and mesh size was manually fine-tuned until no discernible differences appeared in the results (0.04 global seed size). Implicit domain is used since the solid in question was assumed incompressible. Two steps were used for the simulation, the first one was to slide the piston down as the seal is fully made, then a second one where the fluid pressure is applied on the O-ring. Both of the steps used normal, hard contact interaction with the rigid surfaces. Pressure-penetration interaction type was used to simulate the fluid pressurisation.

Contact pressure is not uniform along the O-ring surfaces (as it is shown in Fig. 5). Elements in contact with the surface all have different levels of contact pressure. The circular cross sectional geometry of the undeformed O-ring model produces a maximum contact pressure that is broadly in the middle of the contact area. In order to calculate CoF versus pressure curves, the average contact pressure was used. This average must match the total forces that are present in the nodes in contact with the piston. In Fig. 5, both the individual element value for contact pressure and then an average value over the entire contact surface are shown. The average value is simply calculated as a function of the Abaqus output parameter CFN1 (normal force magnitude of the contact) over the CAREA (contact area) for the model. CFN1 is also used to calculate the normal force of the elastomer acting against the piston.

To confirm the validity of our FEA results, a confirmation was experimentally carried out in the form of an O-ring compression test. Using the curve fit obtained from the uniaxial tension results, an axisymmetric model of an O-ring of the same material was compressed up to 25% of the nominal strain, this was then compared to the results from a simple compression measurement on the O-ring. The instantaneous response was enough for the purpose of this dynamic friction studies, since the piston will cycle up and down, the frictional response is reversed in every half cycle, thus resetting the instantaneous response during each stroke.

Fitting of the measured data to the Yeoh stored energy function was performed using the data fitting algorithm in Abaqus and shows a good fit along the entire testing range (Fig. 8). Data was obtained from uniaxial testing in both tension and compression; for this particular case, the Yeoh model [18] would be the ideal one due to its dependence on the first strain invariant only. There are other, more precise variants of the Yeoh model that can provide better fits at low strain levels [24]. After the Abaqus curve fit, it was observed that the standard Yeoh model was a good enough fit for this work. Yeoh model equation follows:

$$W = C_{10}(I_1 - 3) + C_{20}(I_1 - 3)^2 + C_{30}(I_1 - 3)^3 \quad (3)$$

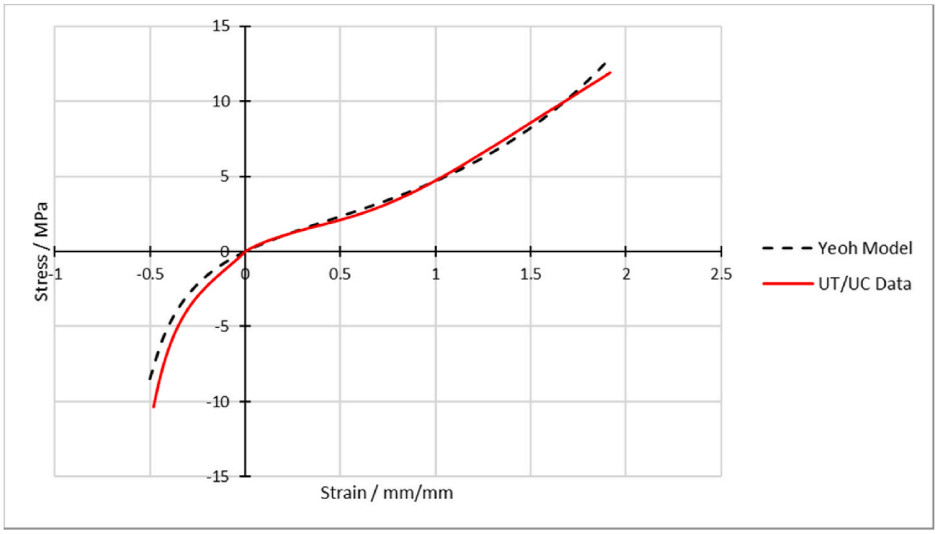

Fig. 8. Uniaxial mechanical testing data with Yeoh fit.

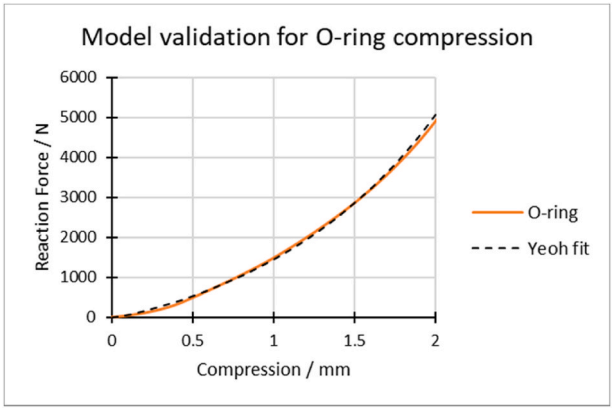

Fig. 9. Force vs. Compression length for the axisymmetric validation experiment.

The derived coefficients for the Yeoh model are: $C_{10} = 1.02$ MPa, $C_{20} = 6.75 \times 10^{-2}$ MPa, $C_{30} = 3.81 \times 10^{-3}$ MPa. In order to validate the model, the compression of an O-ring made of the same elastomer was performed. Even in a simple compression test, the different geometry of the O-ring when compared to a test button was sufficient to provide confidence in the model.

With the previous uniaxial tension fit, we compress the same type of O-ring used in the rig in our validation experiment. Fig. 9 shows a good match between the model and the experiment.

Fig. 10 shows the stress profile of the O-ring when it is compressed in the sleeve glands and then subjected to different levels of fluid pressure. The friction model has little effect on the normal response of the elastomer at higher pressures if a pressure dependent behaviour is used. A simple Thirion [25] model is enough to obtain consistent results. At no point of the experiments was there leakage or breakdown of the O-ring simply arising from the initial pressurisation. No correction for the changes in SEF due to hydrostatic pressure was performed, since it is was assumed that the elastomer behaviour remains largely unchanged in terms of its stress response.

5. Experimental results & discussion

Results from piston surface profile characterisation are presented in Fig. 11. Characterisation of the surface roughness was done in the vertical direction to reflect the piston motion. There is no significant change of surface roughness across the entire length of the piece. Raw data from the profilometer is fitted with the HDC function and a plateau region is identified. The Hurst parameter value for the piston is 0.7. Vertical cut-off and horizontal cut-off lengths are 0.47 and 27 μm respectively. The studied piston was prepared with what appears to be a smooth surface but additional machined pistons with different surfaces and roughness profiles could be prepared and used. All that is required is that piston diameter should be maintained to ensure that the average amount of the precompression in the O-ring remains the same.

As expected, Fig. 12 shows that the CoF reduces with increasing normal pressure. This is well-known and is widely reflected in the literature [22]. The decrease with pressure is further marked under the hydrostatic pressure conditions because silicone oil acts as a lubricant that inhibits the elastomer chains from attaching themselves to the surface. It is worth noting that as the pressure increases, the contact area between the elastomer and the piston surface also increased (Fig. 10). This relation is not directly proportional however, as the contact pressure at its maximum point will increase by a factor of nearly two, whilst the contact area only increases by 30%. This means that the adhesion frictional contribution will not change by much even with the low viscosity of the silicone oil. Still, the increase in contact area cannot be ignored and will be more significant if no lubricant is present. The cavities in the piston surface are filled with lubricant and stop the elastomer from filling the cavities since the liquid is incompressible [27].

The HDC function analysis of the profilometry data gives a value for $\lambda = 27.5$ μm for the machined piston outer sliding surface. Assuming a constant λ across the surface of the piston, we can calculate the frequency of the local deformation of the rubber as V/λ, where the sliding velocity, V, is divided by this characteristic length. With this correlation, we can talk about coefficient of friction that is dependent on frequency rather than speed. Since rubber properties change with frequency of deformation, then a frequency dependent CoF would be more easily translated to different surfaces.

To calculate the actual coefficient of friction (CoF), the experimental value of the sliding force that is extracted from section 5 (Fig. 3) for a given sliding speed is divided by the CFN1 (the normal force obtained using the FEA). The actual face pressure can be obtained by taking the CFN1 value and dividing this by the FEA calculated CAREA value. Fig. 12 highlights in red, the example values measured for 6.89 MPa of fluid pressure, CFN1 = 9978 N, CAREA = 1496 mm^2, showing an average face pressure of the O-ring = 6.67 MPa. The effect of the sliding velocity is also observed in Fig. 12. Since a faster movement of the piston is equivalent to a higher frequency of deformation of the elastomer, a stiffer response is obtained. When a stiffer response occurs, the elastomer has less time to deform into the detailed shape of the micro-grooves that are machined into the piston surface and the resulting local deformation is decreased, causing both lower adhesion and reduced hysteresis.

6. Conclusions

A fully functional friction test methodology that works under hydrostatic pressure conditions has been developed and validated. Results are in accordance with that suggested from comparable data, where available, from the literature. This testing approach opens up several possibilities for characterising a wide range of behaviours and

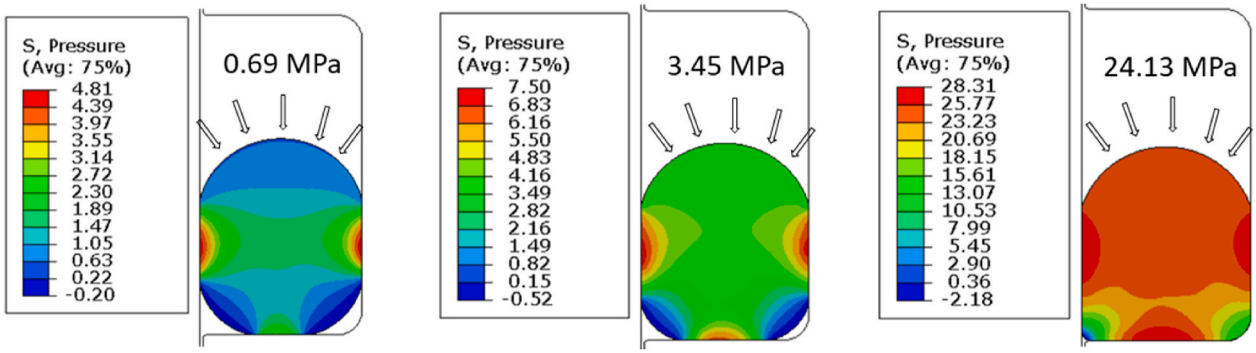

Fig. 10. O-ring axisymmetric model compressed with three different hydrostatic pressure values. Left to right: 0.69, 3.45 and 24.13 MPa.

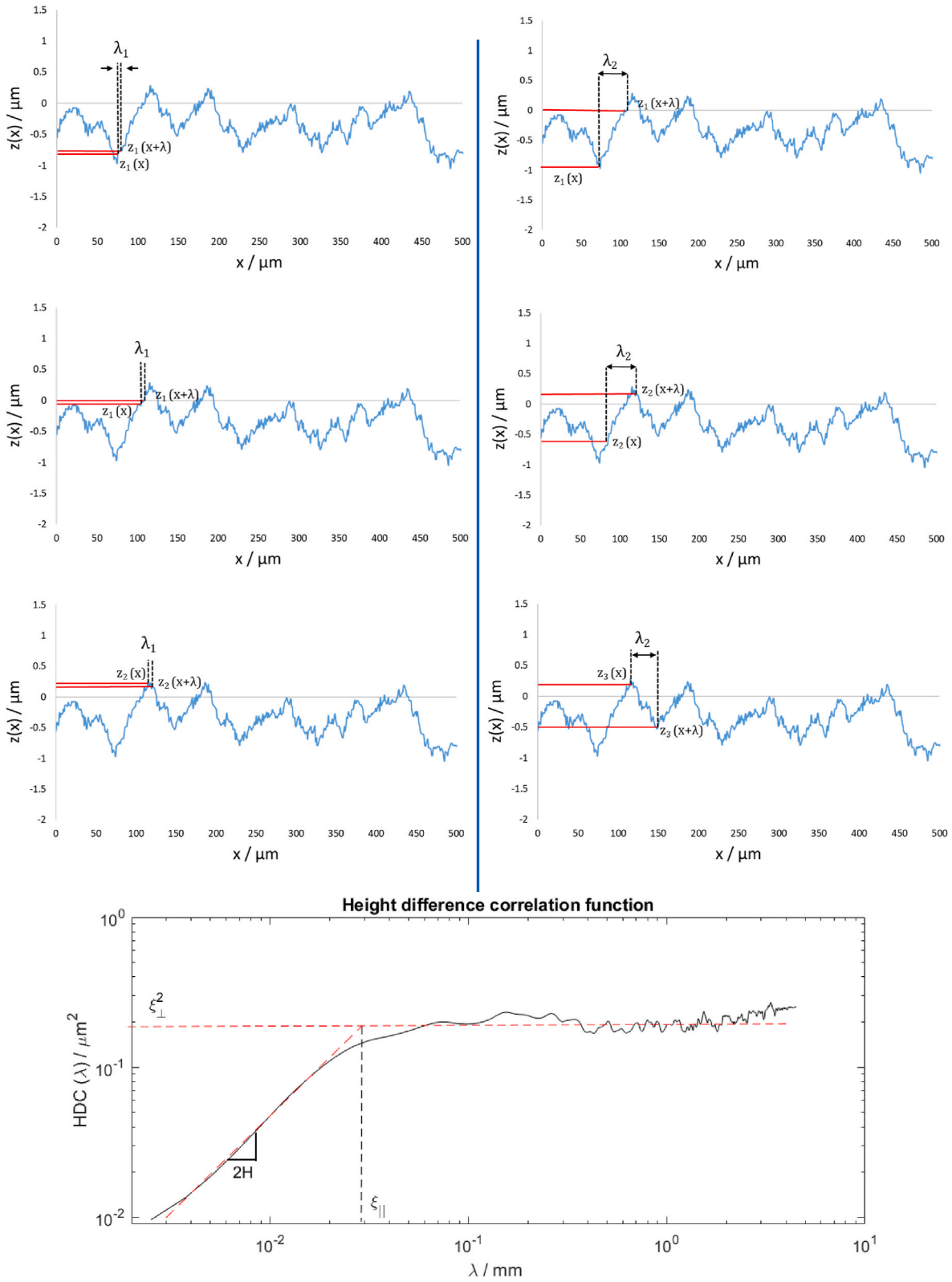

Fig. 11. Raw data from piston profilometry analysed with HDC function. Left side shows the first lambda to be used for analysis across the x-axis. Right side increases the lambda and repeats the previous step. Bottom figure presents the relationship between the lambda value and the correlation function.

dependencies as the rig can work up to 35 MPa pressurisation and is able to operate at high temperatures as well. The effect of surface roughness can be investigated by machining pistons with different surface roughness. Finally the O-ring size elected was an industry standard which means a wide range of different elastomer materials are available for further investigation as well.

Author statement

Eduardo Yanes is the principal researcher who designed and carried

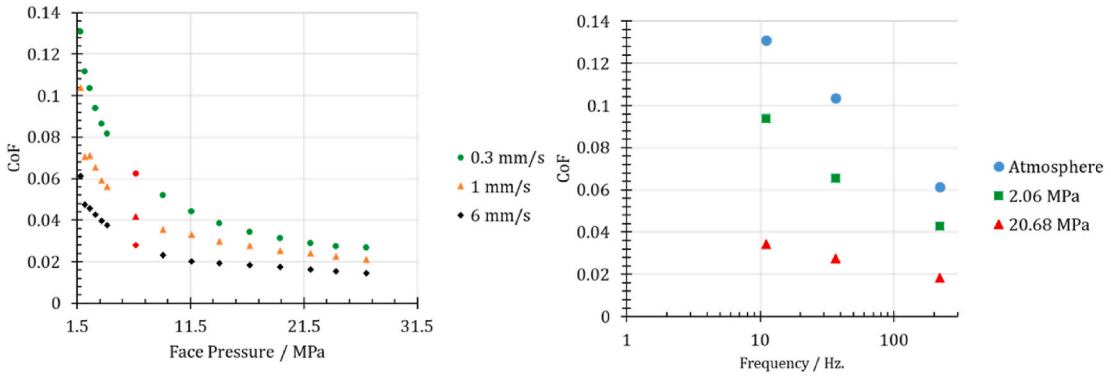

Fig. 12. CoF against contact pressure for six different speed levels, results are then plotted against velocity for three different levels of hydrostatic pressure. Red markers are used on the left hand graph to illustrate the calculations at one particular point of pressure. (For interpretation of the references to colour in this figure legend, the reader is referred to the Web version of this article.)

out the experiments and undertook the data analysis. Benjamin Berryhill works for the project sponsor and helped with the modelling, reviewed the experimental design and assisted with scoping the test rig capabilities. Nicola Pugno is part of the project supervision team and assisted in the data analysis and paper revision. Julien Ramier also works for the project sponsor and was involved in establishing the experimental testing protocols and with the editing of the paper. James Busfield was the principal project supervisor, who secured the project funding, identified the project scope and who was also involved in the experiment design, data analysis and paper revision.

Declaration of competing interest

The authors whose names listed on the paper certify that they have NO affiliations with or involvement in any organization or entity with any financial interest (such as honoraria; educational grants; participation in speakers' bureaus; membership, employment, consultancies, stock ownership, or other equity interest; and expert testimony or patent-licensing arrangements), or non-financial interest (such as personal or professional relationships, affi liations, knowledge or beliefs) in the subject matter or materials discussed in this manuscript.

Acknowledgement

The authors would like to thank Schlumberger limited for financial and technical support of this investigation. Author N.M.P. is supported by the European Commission under LIFE19 ENV/IT/000213 – LIFE GREEN VULCAN.

References

[1] P.C. Pai, D.J. Meier, The effect of pressure on the ultimate properties of elastomers, Rubber Chemistry and Technology 65 (2) (1992) 396–410.
[2] https://www.parker.com/literature/O-Ring%20Division%20Literature/Static%20Files/frictionestimation.pdf.
[3] F.M. Al-Ghathian, M.S. Tarawneh, Friction forces in O-ring sealing, Am. J. Appl. Sci. 2 (3) (2005) 626–632.
[4] P. Gabriel, Investigation And Modelling of Rubber Friction, Doctoral dissertation, 2010.
[5] B.N.J. Persson, Theory of rubber friction and contact mechanics, J. Chem. Phys. 115 (8) (2001) 3840–3861.
[6] B.N.J. Persson, B. Lorenz, M. Shimizu, M. Koishi, Multiscale contact mechanics with application to seals and rubber friction on dry and lubricated surfaces, in: *Designing of Elastomer Nanocomposites: from Theory to Applications*: 103-156, Springer, Cham, 2016.
[7] A. Schallamach, The load dependence of rubber friction, Proc. Phys. Soc. B 65 (9) (1952) 657.
[8] A. Schallamach, A theory of dynamic rubber friction, Wear 6 (5) (1963) 375–382.
[9] O. Galland, E. Holohan, B. van Wyk de Vries, S. Burchardt, Laboratory Modelling of Volcano Plumbing Systems: a Review. Advances in Volcanology, Springer Berlin Heidelberg, 2015, pp. 1–68.
[10] S. Torbruegge, B. Wies, Characterization of pavement texture by means of height difference correlation and relation to wet skid resistance, J. Traffic Transport. Eng. 2 (2) (2015) 59–67.
[11] T. Gredig, E.A. Silverstein, M.P. Byrne, Height-height correlation function to determine grain size in iron phthalocyanine thin films, J. Phys. Conf. 417 (No. 1) (2013) 12069.
[14] P. Thirion, The coefficients of adhesion of rubber, Rubber Chemistry and Technology 21 (2) (1948) 505–515.
[15] O.- Parker, Ring Handbook, 2018.
[16] M. Klüppel, M.M. Moewes, A. Lang, J. Plagge, M. Wunde, F. Fleck, C.W. Karl, Characterization and application of graphene nanoplatelets in elastomers, in: *Designing of Elastomer Nanocomposites: from Theory to Applications*: 319-360, Springer, Cham, 2016.
[18] O.H. Yeoh, Some forms of the strain energy function for rubber, Rubber Chemistry and Technology 66 (5) (1993) 754–771.
[22] D.F. Moore, The Friction and Lubrication of Elastomers, International Series of Monographs on Material Science and Technology, Pergamon Press, Oxford, 1972.
[23] P. Gabriel, A.G. Thomas, J.J.C. Busfield, Influence of interface geometry on rubber friction, Wear 268 (5–6) (2010) 747–750.
[24] T.W. Hohenberger, R.J. Windslow, N.M. Pugno, J.J. Busfield, A constitutive model for both low and high strain nonlinearities in highly filled elastomers and implementation with user-defined material subroutines in ABAQUS, Rubber Chemistry and Technology 92 (4) (2019) 653–686.
[25] P. Thirion, The coefficients of adhesion of rubber, Rubber Chemistry and Technology 21 (2) (1948) 505–515.
[26] B. Lorenz, Y.R. Oh, S.K. Nam, S.H. Jeon, B.N.J. Persson, Rubber friction on road surfaces: experiment and theory for low sliding speeds, J. Chem. Phys. 142 (19) (2015) 194701.
[27] K. Matsuda, D. Hashimoto, K. Nakamura, Real contact area and friction property of rubber with two-dimensional regular wavy surface, Tribol. Int. 93 (2016) 523–529.
[29] B.N.J. Persson, On the theory of rubber friction, Surf. Sci. 401 (3) (1998) 445–454.